Supporting Information

Structural Evidence for Strong Coupling between Polarization Rotation and Lattice Strain in Monoclinic Relaxor Ferroelectrics

Hui Liu,[†] Jun Chen,[†] Longlong Fan,[†] Yang Ren,[‡] Lei Hu,[†] Fangmin Guo,[‡] Jinxia Deng,[†] Xianran Xing[†]*

*Correspondingauthor. junchen@ustb.edu.cn

1. Materials synthesis

The ceramic samples of $0.675Pb(Mg_{1/3}Nb_{2/3})O_3$-$0.325PbTiO_3$ (PMN-PT) were fabricated by a solid-state reaction method using analytic reagent grade oxide powders of PbO, MgO, Nb_2O_5, and TiO_2 (anatase). Firstly, the powder of magnesium niobate were synthesized by calcining homogeneously mixed MgO and Nb_2O_5 powder at 1050 °C for 6 h, and then mixed with PbO and TiO_2. The mixture was hand milled in an agate mortar, which was then calcined at 850 °C for 5 h. Part of calcined powder was pressed into pellets and then sintered at 1250 °C for 2 h covered with the remaining powders to compensate the evaporation loss of PbO. The ceramics were polished and annealed at 500 °C to release stresses. For electric measurements, the ceramic disks with a diameter of 8 mm and a thickness of 1.2 mm were sputtered with gold electrodes. For the in situ high-energy SXRD experiments, the ceramic disks were cut into a bulk shape with dimensions of 1 mm×6 mm×1.2 mm. The gold electrodes were on the two sides of 1 mm×6 mm.

2. In-situ high-energy SXRD experiments

The in-situ high-energy SXRD experiments were performed at 11-ID-C beamline at Advanced Photon Source (APS) at Argonne National Laboratory. The X-ray beam had a spot size of 0.3 mm×0.3 mm, photon energy of about 110 keV and a wavelength of 0.11798 Å. The high energy X-ray penetrated though the ceramic sample. The transmission geometry can well avoid the surface layer effect, which can obtain the real bulk structural information. The diffraction patterns were measured in forward scattering geometry on a Perkin Elmer amorphous silicon area detector which was placed approximately 1800 mm away from the sample. In order to identify the phase structure more clearly, the detector was moved further away from the sample only to collect several

interested diffraction peaks which can alleviate peaks overlapping (Figure S2 and Figure S3d, and the X-ray wavelength was 0.117418 Å). The direction of electric field was perpendicular to the beam line. A bipolar electric field (−3 kV/mm ~ +3 kV/mm) was applied on the sample with a step of about 0.25 kV/mm. Ceria standard was used to calibrate the detector related parameters. The Debye rings were divided into equidistant sectors at 10° intervals to integrate the diffraction intensities, which was performed by the Fit2d software. The detailed schematic of experimental geometry can be seen in Figure 1a of the main text.

3. Macroscopic properties measurements

The macroscopic properties of ferroelectric hysteresis loop (*P*-*E*) and electric field induced strain curve (*S*-*E*) were measured by a ferroelectric tester (model aixACCT, TF Analyzer 1000) at a frequency of 0.5 Hz at room temperature. The piezoelectric coefficient d_{33} was measured by a quasi-static d_{33} meter (China Academy of Acoustics, ZJ-3) after poling the samples under an electric field of 3 kV/mm for 15 min at 60 °C. The measured *P*-*E* and *S*-*E* curves are shown in Figure S1. The saturated polarization is about 36 μC/cm^2 and the coercive field (E_C) is about 0.5 kV/mm. The ceramic samples were well prepared, which can be reflected by the saturated *P*-*E* loop and the high piezoelectric performance (d_{33} = 670±20 pC/N).

4. Data analysis

4.1. Full-profile Rietveld refinements

The detailed crystal structure was refined based on the full-profile Rietveld method performed on the software FULLPROF.[1] Background parameters, scale factor, zero correction, pseudo-Voigt

function profile shape parameters, unit cell parameters, atomic coordinates, and isotropic thermal parameters were refined. Only the isotropic thermal parameters of Pb atom were refined due to the using of hard X-ray and no improvement for using anisotropic thermal parameters.

In the full-profile Rietveld refinements of monoclinic phase with *Cm* space group, set Pb^{2+} as the unit cell origin (0, 0, 0); Ti^{4+}, Nb^{5+}, and Mg^{2+} at (x, 0, z); O_I at the 2*a* sites of (x, 0.5, z), and O_{II} at the 4*b* sites of (x, y, z). The initial atomic coordinates were adopted with the same *Cm* space group of $Pb(Ti,Zr)O_3$.[2]

4.2. Structure analysis details

The crystal structure has been determined by both profile analysis and structure refinement according to the possible structure models such as *P*4*mm*, *R*3*m*, *Cm*, *Bmm*2, and *Pm*.[3] As shown in Figure S3, it is worth noting that monoclinic and tetragonal phases coexistence at unpoled state and low electric field. When applying high electric field, the tetragonal phase is transformed to the monoclinic phase. Once the tetragonal phase is completely transformed to the monoclinic one, the single monoclinic phase is stable even after removing the electric field. It should be noted that the single monoclinic phase stems from the tetragonal phase, which was also observed to the $Pb(Zr_{53.5}Ti_{46.5})O_3$ ceramics.[4] Additionally, it needs to note that the *Cm* model (26) has less fitting parameters than others (34 for *P*4*mm*+*R*3*m*, and 29 for *Pm*). Accordingly, it can be confirmed that the single monoclinic phase (*Cm*) exists for PMN-PT.

4.3. Calculation of polarization and polarization angle (θ)

The polarization (P) was estimated by pure ionic crystal with neglecting the contribution of

electron polarization using Equation (1):

$$P = Z\sum_{i}\frac{\delta z_i q_i}{V} \quad (1)$$

where δz_i is the ion displacements, q_i represents ion charge, V is the unit cell volume and $Z = 1$. The values of δz_i can be calculated by the atomic coordinates according to the refinement results. In a displacive-type perovskite ferroelectric systems, the displacements of A site atoms and the central B site atoms have been taken into consideration to evaluate the polarization vector.[2,4,5,6] According to the Equation (1), the values of P_z and P_{xy} can be calculated, then the magnitude and direction of polarization can be obtained based on the geometric relations. The error bars of θ were estimated from the full-profile Rietveld refinements results according to the error equations.

5. **Strain analysis**

The inter-planar spacing d_{hkl} can be obtained directly from the full-profile Rietveld results. The lattice strain, $\varepsilon_{\mathrm{hkl}}$, of a specific *hkl* lattice plane is calculated by Equation (2):

$$\varepsilon_{\mathrm{hkl}} = \frac{d_{E,\mathrm{hkl}} - d_{0,\mathrm{hkl}}}{d_{0,\mathrm{hkl}}} \quad (2)$$

where d_E and d_0 are the d spacing under an applied electric field and zero electric field, respectively. The error bars in the present study were estimated from the full-profile Rietveld refinements results according to the error equations.

Supplementary Figure and Table

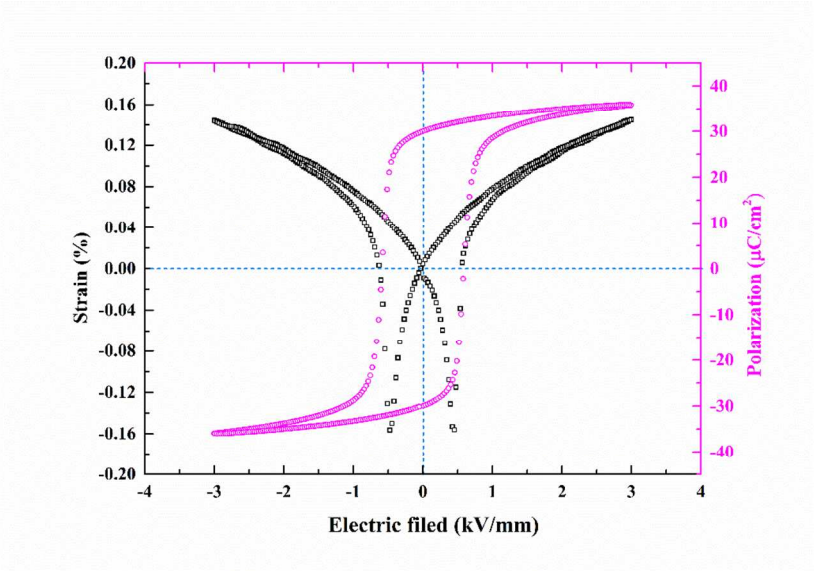

Figure S1. Ferroelectric hysteresis loop (*P*-*E*) and electric-field induced strain curve (*S*-*E*) of PMN-PT ceramics measured at 0.5 Hz at room temperature.

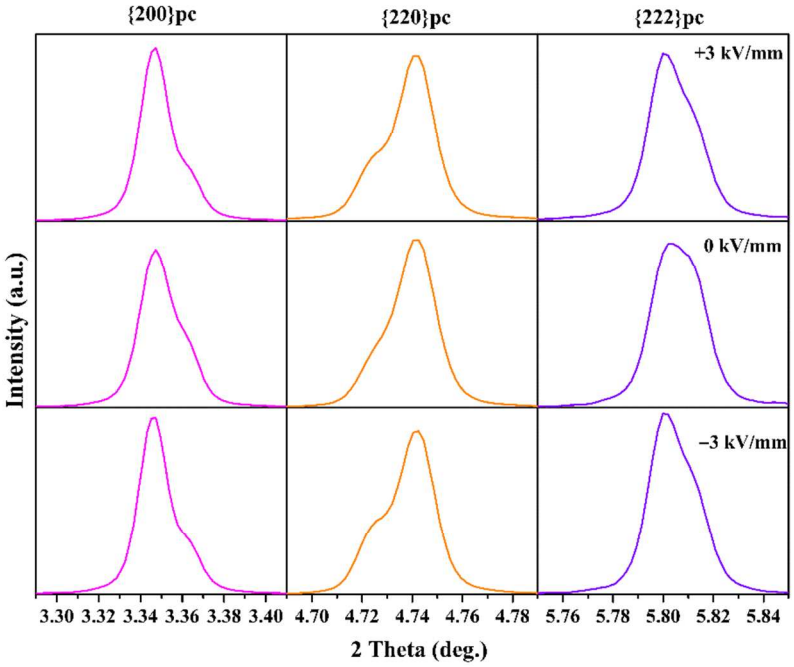

Figure S2. SXRD profiles of $\{200\}_{pc}$, $\{220\}_{pc}$, and $\{222\}_{pc}$ of PMN-PT at various electric fields at the 45° sector.

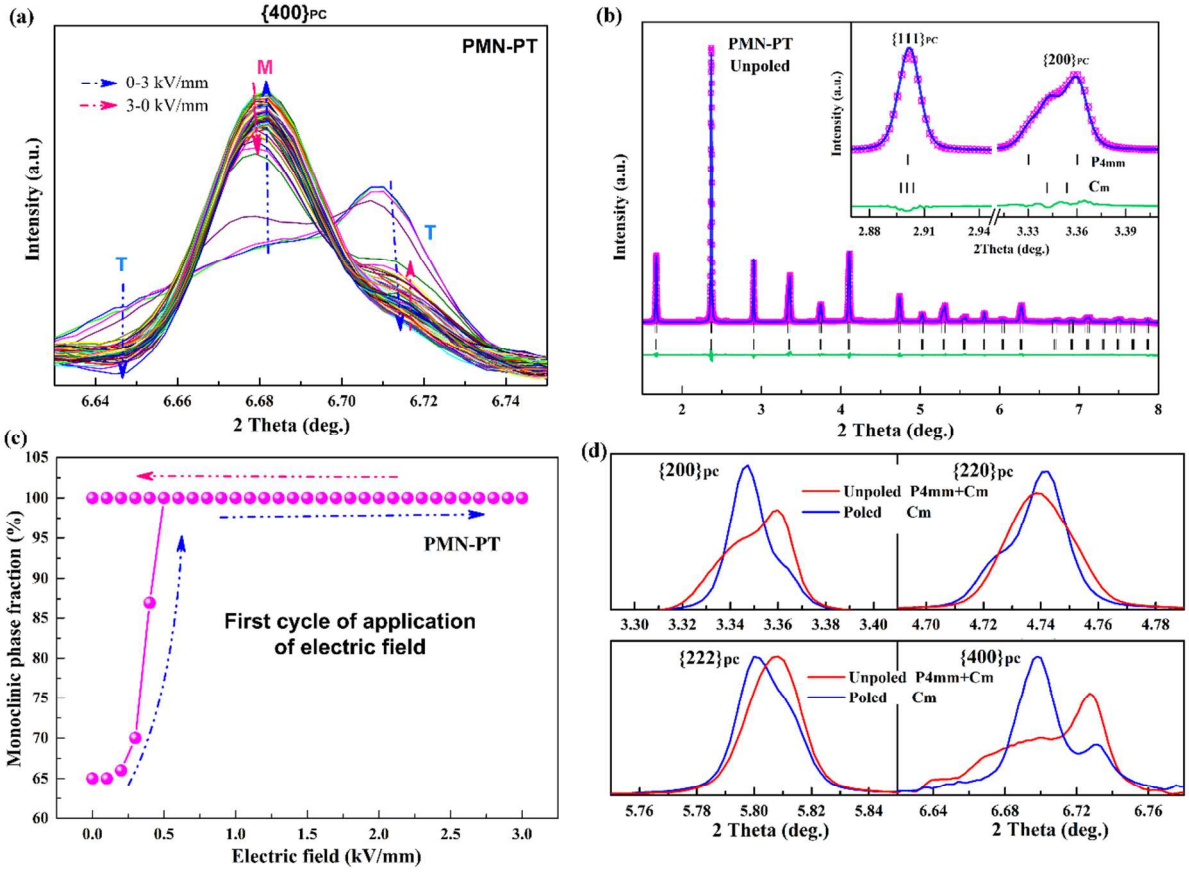

Figure S3. (**a**) The evolution of $\{400\}_{pc}$ at the 45° sector as a function of electric field, (**b**) the full-profile Rietveld refinement results at unpoled state, (**c**) phase fraction of monoclinic phase of PMN-PT as a function of electric field, (**d**) evolution of SXRD profiles of $\{200\}_{pc}$, $\{220\}_{pc}$, $\{222\}_{pc}$, and $\{400\}_{pc}$ for the unpoled and poled PMN-PT ceramics at the 45° sector.

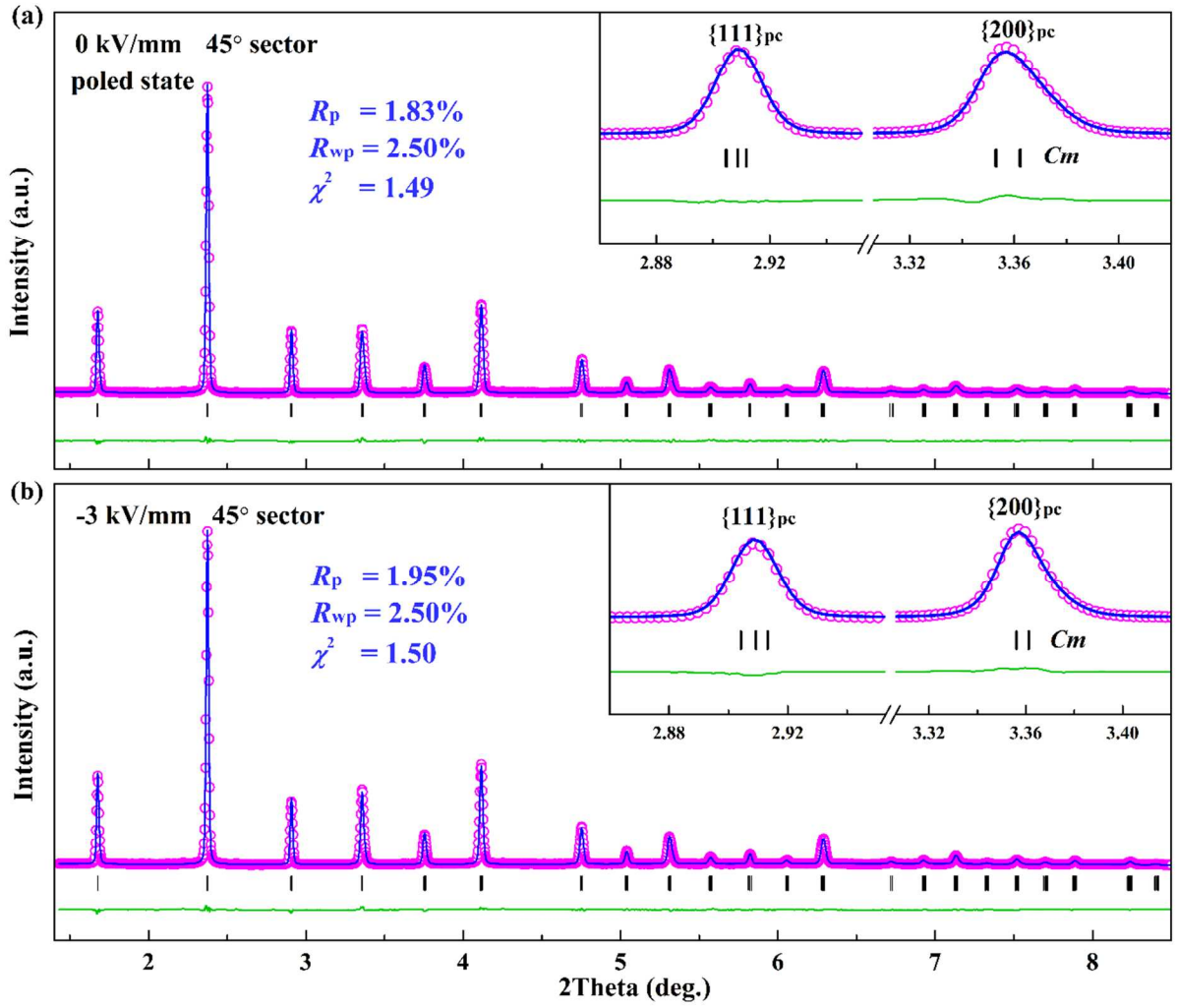

Figure S4. The full-profile Rietveld refinement of monoclinic phase (*Cm*) of PMN-PT. The observed data (pink circle), the calculated profile (blue line), and the difference between the observed and calculated patterns (bottom green line) are depicted. The thick marks indicate the Bragg peak positions of *Cm* model. The inset show the enlarged profile of $\{111\}_{pc}$ and $\{200\}_{pc}$ reflections. (a) at 0 kV/mm (poled state), (b) at −3 kV/mm.

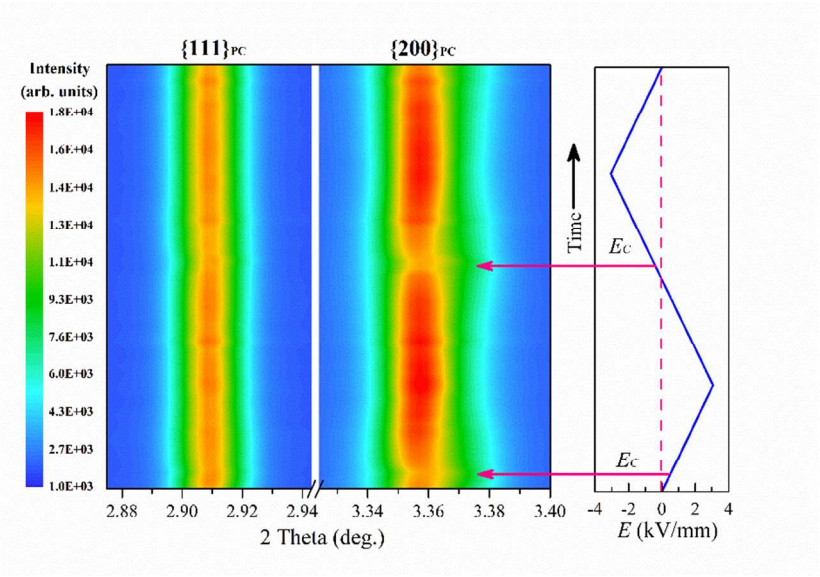

Figure S5. Contour plots of $\{111\}_{pc}$, and $\{200\}_{pc}$ as a function of bipolar electric field for PMN-PT at the 45° sector.

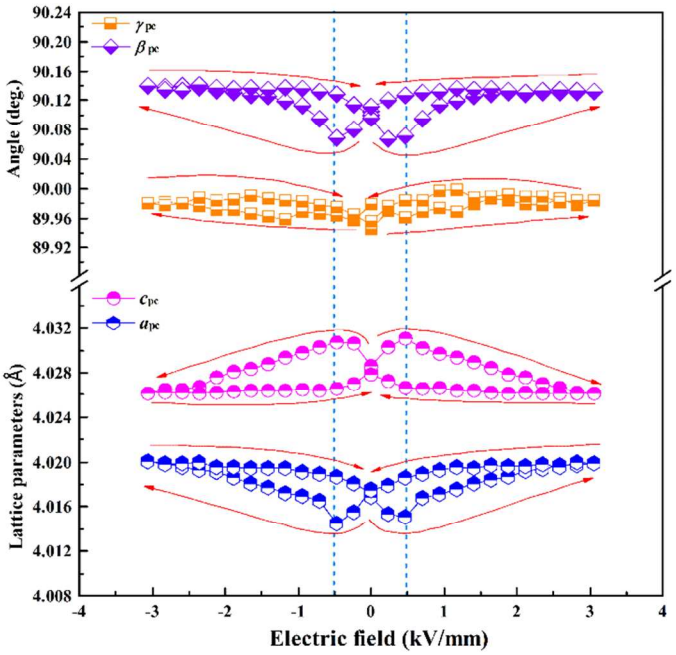

Figure S6. The lattice parameters of perovskite cell as a function of electric field. The perovskite cell parameters were achieved according to the geometrical correlations of $a_{\mathrm{pc}} = \sqrt{a_{\mathrm{m}}^2 + b_{\mathrm{m}}^2}/2, c_{\mathrm{pc}} = c_{\mathrm{m}}$, $\gamma_{\mathrm{pc}} = 2\arctan(b_{\mathrm{m}}/2a_{\mathrm{m}})$, and $\beta_{\mathrm{pc}} = \arccos(\cos\beta_m \cos(\gamma_{\mathrm{pc}}/2))$.

Table S1. The full-profile Rietveld refinement results of the PMN-PT piezoelectric ceramic by using different structural models.

	Zero electric field (poled state)			Max. electric field (+3 kV/mm)		
Space group	R_{wp} (%)	R_p (%)	χ^2	R_{wp} (%)	R_p (%)	χ^2
Cm	2.50	1.83	1.49	2.57	2.03	1.57
Pm	2.75	2.16	1.77	2.76	2.17	1.84
*P*4*mm*	2.90	2.28	1.96	2.82	2.24	1.92
*Bmm*2	2.93	2.29	2.00	2.79	2.21	1.87
*R*3*m*	3.62	2.73	3.06	3.42	2.65	2.82
*P*4*mm*+*R*3*m*	2.69	2.10	1.71	2.70	2.10	1.80

Table S2. Refined structural parameters of PMN-PT with *Cm* model at electric field of 0 kV/mm (poled state) and ±3 kV/mm (the maximum electric field).

		0 kV/mm	−3 kV/mm	+3 kV/mm
a_m (Å)		5.6827(4)	5.6862(2)	5.6858(2)
b_m (Å)		5.6807(4)	5.6842(2)	5.6842(2)
c_m (Å)		4.0286(1)	4.0262(1)	4.0261(0)
β (º)		90.151(4)	90.197(6)	90.187(4)
V (Å^3)		130.05(1)	130.13(1)	130.12(1)
Ti/Nb/Mg	x	0.4868(9)	0.4769(6)	0.4739(9)
	y	0	0	0
	z	0.5417(2)	0.5280(9)	0.5308(7)
O_I	x	0.450(2)	0.497(3)	0.4866(4)
	y	0	0	0
	z	0.097(2)	0.054(5)	0.064(4)
O_{II}	x	0.210(2)	0.172(2)	0.171(1)
	y	0.245(2)	0.235(2)	0.231(1)
	z	0.572(1)	0.531(3)	0.537(2)
$B_{iso(Pb)}$ (Å^2)		2.89(1)	2.69(1)	2.69(1)

References

(1) Rodríguez-Carvajal,J. *Physica B* **1993**, *192*, 55.

(2) Zhang, N.; Yokota, H.; Glazer, A. M.; Ren, Z.; Keen, D. A.; Keeble, D. S.; Thomas, P. A.; Ye, Z. G. *Nat. Commun.* **2014**, *5*, 5231.

(3) Singh,A. K.; Pandey, D.; Zaharko, O. *Phys. Rev. B* **2003**, *68*, 172103.

(4)Fan, L. L.; Chen, J.; Ren, Y.; Pan, Z.; Zhang, L. X.; Xing, X. R. *Phys. Rev. Lett.* **2016**, *116*, 027601.

(5) Haumont, R.; Al-Barakaty, A.; Dkhil, B.; Kiat, J. M.; Bellaiche, L. *Phys. Rev. B* **2005** *71*, 4106.

(6) Carreaud, J.; M.Kiat, J.; Dkhil, B.; Alguero, M.; Ricote, J.; Jimenez, R.; Holc, J.; Kosec., M. *Appl. Phys. Lett.* **2006**, *89*, 252906.